A two-dimensional model for metallic surface roughness resulting from pure waterjet peening

J.Xie[a,*], D.Rittel[a]

[a] *Faculty of Mechanical Engineering, Technion - Israel Institute of Technology, 32000 Haifa, Israel*

Abstract

In implant dentistry, successful osseointegration has been improved by creating a rough surface that increases the available surface area with a consequence of better mechanical cell adhesion compared with smooth surfaces. Pure waterjet peening appears to be a promising technique to achieve controlled surface roughening. In this paper, we analyze a simple case (a full cone shape of waterjet, a flat solid target material, and normal impact). The velocity and pressure spatial distributions of the waterjet are derived based on the liquid impact theory, which helpful for narrowing down the range of process parameters. A 2D axis-symmetric model is used to analyze the deformation behavior of the target material. The performance of 2D analysis is evaluated by comparing with Arola's experimental results (Arola et al., 2001). It shows that the plastic deformation requires a threshold inlet pressure. If the latter reaches the lower limit and keeps increasing, the amount of permanent deformation increases accordingly.

Keywords: Waterjet Peening, Surface Roughness, Finite element modeling

1. Introduction

Pure waterjet peening process, also called abrasiveless waterjet peening, was initially proposed by VanKuiken Jr et al. (VanKuiken Jr et al., 1995) to enhance bonding of thermally sprayed coating. The waterjet roughens the surface to produce a pitted surface with undercuts, so that coating material

*Corresponding author
Email address: jingxie@technion.ac.il (J.Xie)

fills the pits and undercuts to provide a smooth layer of coating material with a strong mechanical/adhesive bond. The waterjet technology concept has been investigated since the early 1960s (Folkes, 2009). It didn't achieve recognition as a viable production tool until M. Hashish devised a new technique consisting of abrasives addition to the waterjet (Hashish, 1984). Since then, the waterjet technology spreads its use to over 50 worldwide industrial sectors, from aerospace and automotive to agriculture and medical industries.

Force water through a narrow orifice with a diameter of 0.08 - 0.8 mm at a high pressure ranging from 140 - 420 MPa, and the water becomes a high velocity jet that can strip, texture or peen the material surface. There are two types of waterjet: pure and abrasive. Abrasive waterjet is similar to a pure waterjet, except that after the pure waterjet is created, abrasive particles, usually garnet, are vacuum pumped into the head and mixed with the water (Hashish et al., 1987). A typical waterjet head is shown in Fig. 1. A wide body of literature on abrasive waterjet machining applications has been published (Arola et al., 2001; Hashish, 1984; Hashish et al., 1987; Lichtarowicz, 2012; Arola and Ramulu, 1997; Momber and Kovacevic, 1998; Ramulu et al., 2000; Osman et al., 2004; Arola et al., 2006; Çaydaş and Hasçalık, 2008; Sadasivam et al., 2009; Wenjun et al., 2011; Anwar et al., 2013), including abrasive waterjet peening process (Arola and McCain, 2000; Arola et al., 2006; Sadasivam et al., 2009). Only few papers are found to deal with surface roughening by pure waterjet peening (Taylor, 1995; Barriuso et al., 2011; Lieblich et al., 2016).

A dental implant is an artificial tooth root that is surgically placed into the jaw bone to hold a replacement tooth. The integration of the dental implant into the surrounding living bone relies on an anchorage mechanism known as "osseointegration" (Shemtov-Yona and Rittel, 2015b). In implant dentistry, successful osseointegration has been improved by creating a rough surface that increases the available surface area with the consequence of better mechanical cell adhesion compared with smooth surfaces (Shemtov-Yona and Rittel, 2014, 2015a, 2016c; Dorogoy et al., 2017; Rittel et al., 2017; De Bruyn et al., 2017). Albrektsson T.(Albrektsson and Wennerberg, 2004) summarized that moderately rough surfaces (Sa between 1.0 and 2.0 μm) show stronger bone responses than smoother or rougher surfaces.

Arola et al. (Arola and McCain, 2000) are the pioneers in the application of abrasive waterjet peening on the surface preparation for metal orthopedic implants. The abrasive waterjet peening is capable of texturing the surface of metal implants trough controlled hydrodynamic erosion. Those authors

Figure 1: A typical waterjet head used for peening.

compared the surface characteristics treated by abrasive and pure waterjet (Arola et al., 2001), and concluded that surface roughness of the metals with pure waterjet peening does not differ significantly from those resulting from abrasive waterjet peening. Approximately 11% (residual) abrasive particles, however, are embedded in the surface of specimen treated by abrasive waterjet (Arola et al., 2006). These embedded particles act as stress concentration points on the surface of the material, which harmful to the fatigue life of medical implants (Shemtov-Yona and Rittel, 2016a,b).

Taylor proposed to roughen the metallic substrates by high pressure pure waterjet in early 1995 (Taylor, 1995). His idea is to erode the substrate in a controlled manner with a minimal thickness loss. Lieblich et al. (Barriuso et al., 2011; Lieblich et al., 2016) analyzed the feasibility and viability of pure waterjet processing for roughening metallic biomaterial Ti6Al4V alloy, and stated two main advantages of this method: high cover rate of area and environment friendly.

In order to predict the surface roughness, researchers have tried various methodologies and strategies to establish cause and effect relationships between process parameters and desired surface characteristics. The main approaches can be classified into four major categories: machining theory, experimental investigation, designed experiments and artificial intelligence (Benardos and Vosniakos, 2003).

Machining theory category includes approaches that place emphasis on certain aspects such as process kinematics, cutting tool properties, chip formation mechanism and so on. With the aid of CAD technique, the creation of the machined surface profile can be simulated by building a geometric model (Lee et al., 2001). The drawback of this approach is that it does not consider several other factors that contribute to the roughness formation mechanism, for example deflection of the cutting tool or certain thermal phenomena.

Experimental investigation is the most conventional approach adopted by researchers, because such experiment-observation-conclusion strategy is the cornerstone of every scientific research activity (Beggan et al., 1999). Does the experiment produce the expected results, and if yes, do the conclusions have universal applicability? The answers of these questions rely on not only the researcher's intuition and insight, but also a deep understanding of the examined phenomenon.

Designed experiments are classified under a different category from the experimental investigation approach is because they constitute a systematic method concerning organizing the experimental procedures and processing data. The response surface methodology (RSM) combing Taguchi techniques is one of the most widespread designed experiments approaches. The RSM investigates how important factors affect the response of an experiment (Wang and Feng, 2002), while Taguchi techniques consist of identifying the most influential parameters and the values that produce the desired output (Nalbant et al., 2007). Due to the strong statistical background of this approach, controlling the size and number of experiments is a crucial issue.

Artificial intelligence (AI) approach imitates the process of information collection by a human, followed by decision making. It is implemented in engineering problems through the artificial neural network (ANN) models (Nalbant et al., 2007), genetic algorithms (GAs) (Suresh et al., 2002), fuzzy logic (Barzani et al., 2015) and expert systems (Iqbal et al., 2007). This approach can offer a possibility for on-line monitoring and/or control of the process. For any AI analyses, there is no need to explicitly formulate the problem, as the code itself can handle the noisy or incomplete data easily. Nevertheless, one of potential hazards is that one cannot guarantee their resulting performance in an application, since all parallel calculations over the neurons are all in a "black box", even the coders themselves cannot tell why the solution algorithm make such and such decisions, especially when more and more neurons are introduced to the algorithm for improving the accuracy.

In this work, we adopt a more "classical" approach based on the identification of the relevant physical parameters of the problem and their introduction into a numerical model. We propose a 2D analysis of waterjet impact problem. The main purpose is to obtain fundamental insights into the characteristic of waterjet, particularly the velocity and pressure distribution in space. We start with a simple case (a full cone shape of waterjet, a flat solid target material, normal impact) and obtain analytic solutions. Next, by comparing with Arola's experimental results (Arola et al., 2001), the performance of 2D analysis is evaluated. It turns out that the results from 2D analysis are only partly satisfactory, so that the approach is extended to a full 3D analysis reported in another paper.

In section 2, the general features of waterjet are described, and three basic assumptions are listed for a successful analysis. In section 3, the waterjet impact problem is formulated step by step, and the analytic solution of pressure distribution is applied to the finite element model as an external load, and along with 2D axis-symmetric boundary conditions, the deformation behavior of the target material are analyzed and discussed.

2. General features of waterjet

Waterjet peening is a versatile machining process. The versatility is embodied in a variety of spray nozzles, for example, twin fluid, swirl, hydraulic, ultrasonic, rotary, electrostatic nozzles, etc.(Ashgriz, 2011, chapter 10). Each of them is designed to generate the desired droplet size and velocity distribution for a special application.

For a typical waterjet peening, the Reynolds number is greater than 3000, indicating that the waterjet used for peening process is a fully turbulent jet. Generally speaking, for a turbulent waterjet, there are three regions as shown in Fig. 2 the initial (region I), main (region II), and final region. (The abbreviations of the region I and II are maintained throughout the paper except otherwise mentioned.) Region I is typically used for cutting, stripping and removal of unwanted coating or material due to the higher kinetic energy of waterjet; consequently, cleaning, optimization of coating adherence, and peening mostly occurs in region II; the final region is not feasible as it has dissipated too much energy to effectively modify the surface or subsurface of a material (Chillman et al., 2009).

Thanks to the development of computing power, more and more researchers could establish the reliability of the numerical simulations from dif-

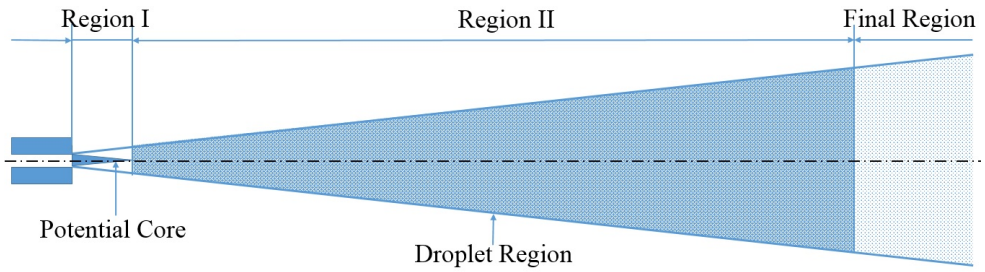

Figure 2: Schematic diagram of waterjet in the air.

ferent perspectives (Wenjun et al., 2011; Chillman et al., 2009; Yoon et al., 2004; Kunaporn et al., 2003; Rajesh and Ramesh Babu, 2006; Maniadaki et al., 2007; Ma et al., 2008; Guha et al., 2011; Shinjo and Umemura, 2011; Hsu et al., 2013). In this work, we start from the simple 2D model, since using the minimum computational resource to maximize the simulation performance is a key principle that should be respected.

- The simplest case of a pure waterjet is that of a steady state waterjet with a full cone spray shape impinging perpendicular to the substrate.
- The target material is simplified as a semi-infinite deformable solid plate with a (clean) flat surface.
- Break-up and atomization of the waterjet are not considered at this stage since the present investigations are mainly confined to the roughening of substrate surface instead of the waterjets behavior.

3. 2D Analysis

3.1. Problem formulation

Waterjet peening is a modified shot peening process (Kumar et al., 2013) because it uses a high-pressure waterjet instead of high velocity solid shots. Hertzian pressure distribution is used to represent the contact pressure resulting from the impact of the solid shot. Compared with established research on shot peening, waterjet peening still lacks a firm theoretical basis to define the pressure distribution at the impacted surface. Field et al. (Field and Lesser, 1977; Lesser and Field, 1983; Obara et al., 1995; Field, 1999) developed a theory for liquid impact on surfaces. For liquid impact on a rigid target, the contact pressure, frequently referred to as the "water-hammer" pressure, is:

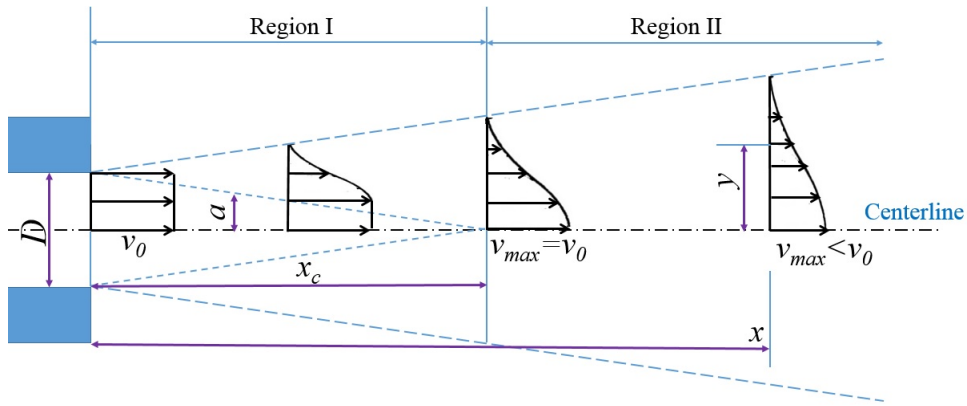

Figure 3: Schematic Representation of waterjet diffusion.

$$P_c = \rho V C_1 \tag{1}$$

where ρ is the density of water, V is the impact velocity of waterjet and C_1 is the shock velocity of water.

The shock velocity of water C_1 can be determined from the relation:

$$C_1 = C_0 + kV \tag{2}$$

where C_0 is the acoustic velocity of water (around 1476 m/s), and k is a constant, close to 2 for water in the velocity range up to 1000 m/s.

Combing Eq. 1 and 2, one can note that the contact pressure is a function of the impact velocity of the the waterjet. Gauntner et al. (Gauntner et al., 1970) gave a comprehensive review of the impact velocity profile of waterjet at different regions. Fig. 3 depicts schematically the impact velocity distribution of a round waterjet in regions I and II, where v_0 and v_{max} stand for the nozzle exit velocity and the maximum velocity, respectively; x and y stand for the distance along the axial and radial direction, respectively; D is the nozzle exit diameter. Inside the potential core of region I, the velocity equals to nozzle exit velocity v_0 everywhere; outside the potential core, it follows the general trend of a Gaussian distribution. When waterjet spreads into region II, the centerline (maximum) velocity declines linearly, while just as in region I, the radial velocity can be described by a Gaussian distribution.

The velocity can be expressed as below:

$$v(0 < x \leq x_c, 0 < y \leq a) = v_0 \tag{3}$$

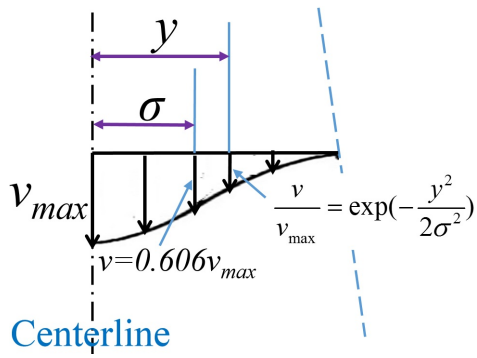

Figure 4: Characteristics of Gaussian distribution of velocity.

$$v(0 < x \leq x_c, y > a) = v_0 exp[-\frac{(y-a)^2}{2\sigma_1^2}] \tag{4}$$

$$v(x > x_c, y) = (1 - \frac{mx}{D}) exp(-\frac{y^2}{2\sigma_2^2}) \tag{5}$$

where x_c and a are the potential core length and radius, respectively. Note that $a = 0.5D(1 - x/x_c)$; σ_1 and σ_2 are the standard deviations (the value of y for which $v = 0.606v_{max}$; see Fig. 4) for region I and region II, respectively; m is a slope constant.

According to Rajaratnam et al. (Rajaratnam et al., 1994), the maximum velocity remains constant and equals to v_0 for more than $100D$ and decays linearly to about $0.25v_0$ at about $2500D$:

$$v(0 < x \leq x_c, 0) = v_0 \tag{6}$$

$$0.25v_0 = (1 - 2500D \times \frac{m}{D})v_0 \tag{7}$$

Consequently, the potential core length $x_c = 100D$ was used under a conservative consideration and the value of slope m is 0.0003 after solving Eq. 7.

Up to now, only one parameter is left to be determined, namely the nozzle exit velocity v_0. One can ignore the pressure variation of the waterjet in the nozzle and consider it as an incompressible flow, thus based on the Bernoulli's principle:

$$v_0 = \sqrt{\frac{2P_{in}}{\rho}} \tag{8}$$

where P_{in} is the inlet pressure of nozzle.

Hence, using Eq. 1 to 8, the contact pressure profile P_c can be expressed as a piecewise function:

$$P_c(0 < x \leq x_c, 0 < y \leq a) = \rho v_0(C_0 + 2v_0) \tag{9}$$

$$P_c(0 < x \leq x_c, y > a) = \rho v_0 C_0 exp[-\frac{(y-a)^2}{2\sigma_1^2}] + 2\rho v_0^2 exp[-\frac{(y-a)^2}{\sigma_1^2}] \tag{10}$$

$$P_c(x > x_c, y) = (1 - \frac{mx}{D})[\rho v_0 C_0 exp(-\frac{y^2}{2\sigma_2^2}) + 2\rho v_0^2 exp(-\frac{y^2}{\sigma_2^2})] \tag{11}$$

where $a = 0.5D - 0.005x$ and $m = 0.0003$.

3.2. Finite element model

A biocompatible titanium base alloy that is suitable for bone implant should have good workability and ductility(Oldani and Dominguez, 2012). The implant material should also have a high yield strength and fatigue strength to sustain cyclic loading. Ti6Al4V, a common implant metallic material, exhibits all those features. Therefore, an elastic-plastic nonlinear finite element analysis was performed using the commercial software Abaqus/Explicit, version 6.14 (Abaqus, 2014). The two-dimensional semi-infinite geometry was created to simulate the area under and near the axis-symmetric body of the target plate. The material properties of Ti6Al4V (Dorogoy and Rittel, 2009) for this FE analysis are listed in Table 1. An isotropic hardening model available in Abaqus software accounting for the elastic-plastic behavior of material was used. Note here that, no matter whether kinematic, isotropic, or perfectly plastic, or even mixed hardening law, their influence on the final results didn't show considerable difference (Taro et al., 2015).

The mesh structure and model dimension is shown in Fig. 5. In total, this 2D model contains 11584 nodes and 11340 CAX4R elements (A 4-node bilinear axisymmetric quadrilateral, reduced integration, hourglass control).

Table 1: The material properties of Ti6Al4V.

Material	Ti6Al4V
Youngs Modulus, E(Pa)	1.14×10^{11}
Poissons ratio, ν	0.342
Yield stress, σ_y (Pa)	880×10^6
Density, ρ (Kg/m^3)	4.43×10^3

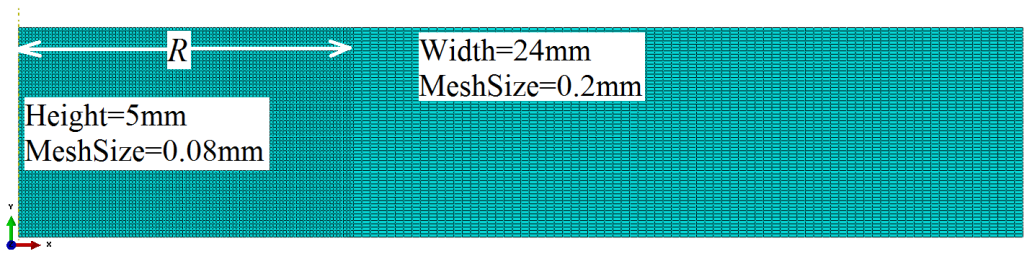

Figure 5: Mesh structure of 2D axis-symmetric model.

This mesh density was chosen to keep the number of elements and the computational time within a reasonable range.

Arola et al.'s experimental results were chosen as a reference to evaluate the 2D model (Arola et al., 2001). In their experiments, the diameter of nozzle exit is 0.9 mm, and the pure waterjet peening is held constant at 150 mm ($x > 100D$,region II), which resulted in the maximum waterjet radius R at impingement of approximately 8 mm (Arola et al., 2001). According to that, the dimension of the target plate is width=$3R$=24 mm, and height=5 mm. The vertical boundary of the mesh was constrained against displacement in the x-direction, and the bottom boundary against displacement in all directions. Because of the dynamic similarity at all cross sections of waterjet ($\sigma/x = cons.$), the velocity distribution by assuming the $v/v_{max} = 0.001$ at the maximum radius of waterjet could be written as:

$$v(x, y) = (1 - \frac{0.0003x}{D})v_0 exp(-2428.5\frac{y^2}{x^2}) \tag{12}$$

Using Eq. 12 in evaluating Eq. 11 yields the pressure profile relating the shock velocity of waterjet:

$$\frac{P_c(x,y)}{P_c(x,0)} = \frac{C_1(x,y)}{C_1(x,0)} exp(-2428.5\frac{y^2}{x^2}) \tag{13}$$

Therefore, for a full cone shape of waterjet ejecting from a nozzle with a diameter of 0.9 mm, its velocity distribution and pressure distribution normalizing to the maximum velocity and the maximum pressure along the radial direction are shown in Fig. 6, respectively. The normalized pressure distribution seems also follow the exponent form, the Eq. 13 thus could be fitted again for simplicity and becomes (Adjusted R-square=0.9998):

$$\frac{P_c(x,y)}{P_c(x,0)} = exp(-2965.5\frac{y^2}{x^2}) \tag{14}$$

The pressure calculated using Eq. 14 was applied directly as a surface pressure on the nodes of top layer elements. The phenomenon of pressure stages (water hammer pressure stage and stagnation pressure stage) arising from the liquid impact mechanism (Field, 1999) can be realized by loading (step 1) and unloading (step 2) linearly in 10 increments, respectively. The permanent deformation could thus be evaluated by this simplified analysis.

3.3. Result and discussion

For the case 14 of Arola et al.'s experiments (Arola et al., 2001), in which the inlet pressure is 210 MPa and the standoff distance (SOD) is 150 mm, the maximum equivalent plastic strain is 0.33% according to our simulation results (Fig. 7(a)). For 140 MPa inlet pressure, no plastic deformation occurred at the target material; but higher plastic deformation up to 1.25% and larger yield region were found beneath the material surface for 280 MPa case. The material surface subjected to a waterjet peening process undergoes local plastic deformation. The plastically deformed regions undergo permanent deformation and the surface geometry is modified as shown in Fig. 7(b). Note that the deformation was zoomed in 100 times to make a clearer presentation. The maximum vertical displacements ($U2$) with different inlet pressures predicted by using 2D model are compared with the arithmetic average roughness (R_a) and peak to valley height (R_v) measured by Arola et al. (Arola et al., 2001), and from Tab. 2 one can draw three qualitative conclusions.

The inlet pressure 140 MPa has no considerable influence on the plastic deformation of the target material, as shown both experimentally and numerically. In Arola's experiments, although the R_a of target material did

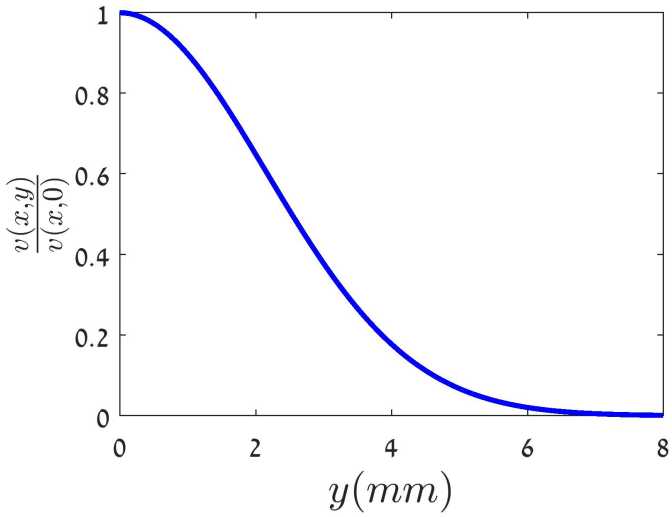

(a)

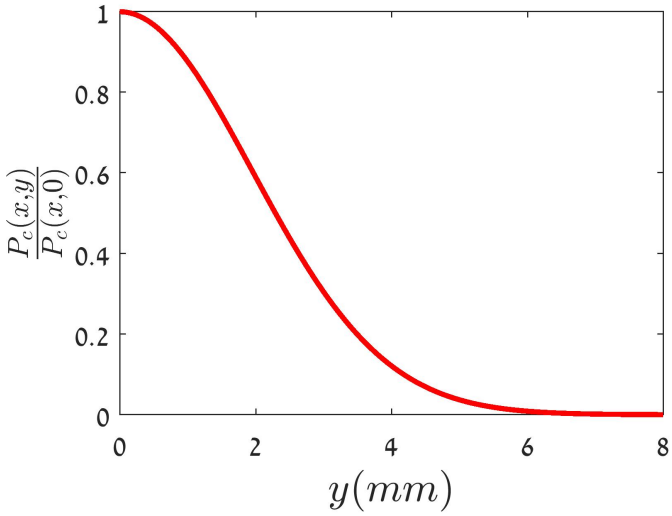

(b)

Figure 6: (a) Normalized velocity distribution and (b) normalized pressure distribution along radial direction of waterjet at the location of standoff distance 150 mm.

increase from 0.9 μm to 1 μm under 140 MPa pressure, the change is insignificant compared to case of 210 MPa and 280 MPa, which increased the R_a by more than two times. The simulation results of $U2$ show a negligible increase from 0 to 4.8×10^{-3} μm for 140 MPa case. The surface was assumed to be flat without any initial roughness condition in the simulation. This may explain the discrepancy between the numerical and experimental results.

The maximum $U2$ is a global measurement of plastic deformation, and its value should lie between R_a and R_v, where R_a and R_v can be seen as the minimum and maximum global deformation of target surface, respectively. The maximum $U2$ values of 280 MPa and 210 MPa cases indeed fall into their individual $[R_a,\ R_v]$ range. The inconsistency of 140 MPa cases is due to the flat surface assumption. This can be qualitatively justified based on the fact that when the effect of roughening is comparable to the initial surface roughness, the latter becomes more important than in the case of a significant surface roughening that exceeds noticeably the initial surface roughness. In the future we intend to exclude the flat surface assumption and include an initial surface roughness condition that will compensate the inadequacy of 140 MPa case and enhance the prediction ability for higher pressure cases at the same time.

The third conclusion is that an increase in inlet pressure causes an increase in average plastic deformation, as expected. From the second column of Tab. 2, the simulation results show a continuous rise on the deflection of target surface along with the increase of inlet pressure. R_a and R_v show the same trend, but the rate of increase is different. In order to quantitatively calculate R_a and R_v, one needs to "generate" peaks and valleys, which means the surface roughness profile. The smooth curve obtained in this study cannot provide such detail information of surface, so that a more elaborate approach is required, as described in our next paper on this topic (Xie and Rittel, 2017).

The 2D numerical analysis developed in this study has an attractive advantage for researchers and engineers who wish to obtain a ballpark range of inlet pressure or standoff distance for a desired surface roughness. For example, if someone wants to obtain a 2.2 μm surface roughness, then at a standoff distance of 150 mm, the inlet pressure must be higher than 210 MPa. Based on the velocity distribution (Eq. 3 to 5) and pressure distribution (Eq. 9 to 11) derived in the section 3.1, the rough range of standoff distance for a given inlet pressure or the rough range of inlet pressure for a given standoff distance or a series of combination of velocity and pressure could be achieved only by a few simple and fast 2D simulations. This will

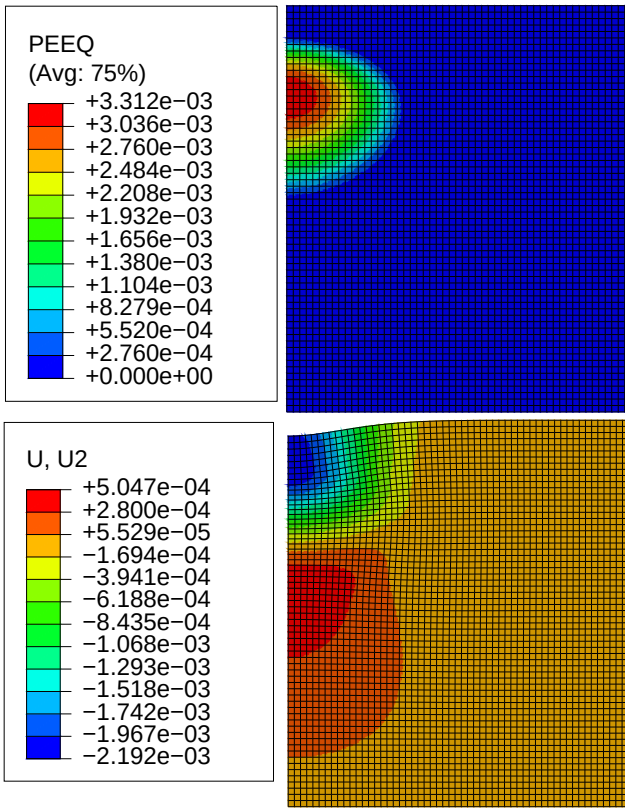

Figure 7: Contours of (a) equivalent plastic strain and (b) y-axis displacement of target material after the waterjet peening (Pin=210 MPa, SOD=150 mm).

narrow down the range of process parameters and make a good preparation for the fine optimization stage.

2D numerical analysis can be used as a feasible tool for prediction of residual stresses as well. The residual stress resulting from the same case 14 (P_{in}=210 MPa, SOD=150 mm) by experimental measurement is 93±40 MPa, the predicted value is 74 MPa which within the experimental range. Moreover, it can provide the residual stresses distribution both in depth and width direction. This part will be discussed in a future paper.

4. Conclusions

In this paper, a theoretical and numerical framework is established to predict the metallic surface roughness resulting from pure waterjet peening.

Table 2: Comparison of Simulation and Experimental results of roughness.

P_{in}(MPa)	Simulation results	Experimental results (Arola et al., 2001)	
	$U2_{max}(\mu m)$	$R_a(\mu m)$	$R_v(\mu m)$
280	15.3	2.4	17.9
210	2.2	2.2	23.0
140	4.8×10^{-3}	1.0	8.6
Substrate	0	0.9	9.8

A 2D finite element model is used to investigate the deformation behavior of the flat target material under the impingement of a full cone shape of waterjet. Calculated pressure distribution according to the liquid impact theory is applied directly as a surface pressure on the nodes of top layer elements.

The surface geometry of target material is modified due to the effect of local plastic deformation. Plastic deformation must be triggered by sufficient inlet pressure, otherwise no considerable geometry change observed on the target material surface. If the inlet pressure reaches the lower limit and keeps increasing, the amount of permanent deformation is increasingly larger. The origin surface roughness affects the successful prediction and should be considered in the simulation.

The 2D model can narrow down the range of process parameters and save the time and cost of researchers for a fine optimization of waterjet operation process.

Yet, the 2D model is limited in its ability to reproduce or predict the actual surface roughness resulting from the impact of myriads of droplets on a solid metallic surface. Additional work is needed to address this issue.

Acknowledgement

The work is supported in part at the Technion by a Technion-Guangdong Fellowship. Thanks for the enthusiastic help from all the colleagues of Dynamic Fracture Laboratory of Technion Israel Institute of Technology.

References

Abaqus, V., 2014. 6.14 documentation. Dassault Systemes Simulia Corporation.

Albrektsson, T., Wennerberg, A., 2004. Oral implant surfaces: Part 1–review focusing on topographic and chemical properties of different surfaces and in vivo responses to them. International Journal of Prosthodontics 17 (5).

Anwar, S., Axinte, D., Becker, A., 2013. Finite element modelling of overlapping abrasive waterjet milled footprints. Wear 303 (1), 426–436.

Arola, D., Alade, A., Weber, W., 2006. Improving fatigue strength of metals using abrasive waterjet peening. Machining science and technology 10 (2), 197–218.

Arola, D., McCain, M. L., Kunaporn, S., Ramulu, M., 2001. Waterjet and abrasive waterjet surface treatment of titanium: A comparison of surface texture and residual stress. Wear 249 (10-11), 943–950.

Arola, D., Ramulu, M., 1997. Material removal in abrasive waterjet machining of metals surface integrity and texture. Wear 210 (1-2), 50–58.

Arola, D. D., McCain, M. L., 2000. Abrasive waterjet peening: A new method of surface preparation for metal orthopedic implants. Journal of biomedical materials research 53 (5), 536–546.

Ashgriz, N., 2011. Handbook of atomization and sprays: theory and applications. Springer Science & Business Media.

Barriuso, S., Lieblich, M., Multigner, M., Etxeberria, I., Alberdi, A., González-Carrasco, J. L., 2011. Roughening of metallic biomaterials by abrasiveless waterjet peening: Characterization and viability. Wear 270 (9), 634–639.

Barzani, M. M., Zalnezhad, E., Sarhan, A. A., Farahany, S., Ramesh, S., 2015. Fuzzy logic based model for predicting surface roughness of machined al–si–cu–fe die casting alloy using different additives-turning. Measurement 61, 150–161.

Beggan, C., Woulfe, M., Young, P., Byrne, G., 1999. Using acoustic emission to predict surface quality. The International Journal of Advanced Manufacturing Technology 15 (10), 737–742.

Benardos, P., Vosniakos, G.-C., 2003. Predicting surface roughness in machining: a review. International journal of machine tools and manufacture 43 (8), 833–844.

Çaydaş, U., Hasçalık, A., 2008. A study on surface roughness in abrasive waterjet machining process using artificial neural networks and regression analysis method. Journal of materials processing technology 202 (1), 574–582.

Chillman, A., Ramulu, M., Hashish, M., 2009. A general overview of waterjet surface treatment modeling. In: American WJTA Conference and Expo.

De Bruyn, H., Christiaens, V., Doornewaard, R., Jacobsson, M., Cosyn, J., Jacquet, W., Vervaeke, S., 2017. Implant surface roughness and patient factors on long-term peri-implant bone loss. Periodontology 2000 73 (1), 218–227.

Dorogoy, A., Rittel, D., 2009. Determination of the johnson–cook material parameters using the scs specimen. Experimental mechanics 49 (6), 881.

Dorogoy, A., Rittel, D., Shemtov-Yona, K., Korabi, R., 2017. Modeling dental implant insertion. Journal of the Mechanical Behavior of Biomedical Materials 68, 42–50.

Field, J., 1999. Elsi conference: invited lecture: liquid impact: theory, experiment, applications. Wear 233, 1–12.

Field, J., Lesser, M., 1977. On the mechanics of high speed liquid jets. In: Proceedings of the Royal Society of London A: Mathematical, Physical and Engineering Sciences. Vol. 357. The Royal Society, pp. 143–162.

Folkes, J., 2009. Waterjetan innovative tool for manufacturing. Journal of Materials Processing Technology 209 (20), 6181–6189.

Gauntner, J. W., Hrycak, P., Livingood, J., 1970. Survey of literature on flow characteristics of a single turbulent jet impinging on a flat plate.

Guha, A., Barron, R. M., Balachandar, R., 2011. An experimental and numerical study of water jet cleaning process. Journal of Materials Processing Technology 211 (4), 610–618.

Hashish, M., 1984. A modeling study of metal cutting with abrasive waterjets. Journal of Engineering Materials and Technology 106 (1), 88–100.

Hashish, M. A., Kirby, M. J., Pao, Y.-H., Mar. 10 1987. Method and apparatus for forming a high velocity liquid abrasive jet. US Patent 4,648,215.

Hsu, C.-Y., Liang, C.-C., Teng, T.-L., Nguyen, A.-T., 2013. A numerical study on high-speed water jet impact. Ocean Engineering 72, 98–106.

Iqbal, A., He, N., Li, L., Dar, N. U., 2007. A fuzzy expert system for optimizing parameters and predicting performance measures in hard-milling process. Expert Systems with Applications 32 (4), 1020–1027.

Kumar, H., Singh, S., Kumar, P., 2013. Modified shot peening processes–a review. International Journal of Engineering Sciences & Emerging Technologies 5 (1), 12–19.

Kunaporn, S., Ramulu, M., Jenkins, M. G., Hashish, M., 2003. Residual stress induced by waterjet peening: A finite element analysis. In: ASME 2003 Pressure Vessels and Piping Conference. American Society of Mechanical Engineers, pp. 5–13.

Lee, K. Y., Kang, M. C., Jeong, Y. H., Lee, D. W., Kim, J. S., 2001. Simulation of surface roughness and profile in high-speed end milling. Journal of Materials Processing Technology 113 (1), 410–415.

Lesser, M., Field, J., 1983. The impact of compressible liquids. Annual review of fluid mechanics 15 (1), 97–122.

Lichtarowicz, A., 2012. Jet cutting technology. Vol. 13. Springer Science & Business Media.

Lieblich, M., Barriuso, S., Ibáñez, J., Ruiz-de Lara, L., Díaz, M., Ocaña, J., Alberdi, A., González-Carrasco, J. L., 2016. On the fatigue behavior of medical ti6al4v roughened by grit blasting and abrasiveless waterjet peening. Journal of the mechanical behavior of biomedical materials 63, 390–398.

Ma, L., Bao, R.-h., Guo, Y.-m., 2008. Waterjet penetration simulation by hybrid code of sph and fea. International Journal of Impact Engineering 35 (9), 1035–1042.

Maniadaki, K., Kestis, T., Bilalis, N., Antoniadis, A., 2007. A finite element-based model for pure waterjet process simulation. The International Journal of Advanced Manufacturing Technology 31 (9), 933–940.

Momber, A. W., Kovacevic, R., 1998. Principles of abrasive water jet machining. Springer Science & Business Media.

Nalbant, M., Gökkaya, H., Sur, G., 2007. Application of taguchi method in the optimization of cutting parameters for surface roughness in turning. Materials & design 28 (4), 1379–1385.

Obara, T., Bourne, N., Field, J., 1995. Liquid-jet impact on liquid and solid surfaces. Wear 186, 388–394.

Oldani, C., Dominguez, A., 2012. Titanium as a biomaterial for implants. In: Recent Advances in Arthroplasty. InTech.

Osman, A., Mabrouki, T., Thery, B., Buisine, D., 2004. Experimental analysis of high-speed air–water jet flow in an abrasive water jet mixing tube. Flow Measurement and Instrumentation 15 (1), 37–48.

Rajaratnam, N., Rizvi, S., Steffler, P., Smy, P., 1994. An experimental study of very high velocity circular water jets in air. Journal of Hydraulic Research 32 (3), 461–470.

Rajesh, N., Ramesh Babu, N., 2006. Multidroplet impact model for prediction of residual stresses in water jet peening of materials. Materials and manufacturing processes 21 (4), 399–409.

Ramulu, M., Kunaporn, S., Arola, D., Hashish, M., Hopkins, J., 2000. Waterjet machining and peening of metals. Journal of Pressure Vessel Technology 122 (1), 90–95.

Rittel, D., Dorogoy, A., Shemtov-Yona, K., 2017. Modelling dental implant extraction by pullout and torque procedures. Journal of the Mechanical Behavior of Biomedical Materials 71, 416–427.

Sadasivam, B., Hizal, A., Arola, D., 2009. Abrasive waterjet peening with elastic prestress: A parametric evaluation. International Journal of Machine Tools and Manufacture 49 (2), 134–141.

Shemtov-Yona, K., Rittel, D., 2014. Identification of failure mechanisms in retrieved fractured dental implants. Engineering Failure Analysis 38, 58–65.

Shemtov-Yona, K., Rittel, D., 2015a. On the mechanical integrity of retrieved dental implants. journal of the mechanical behavior of biomedical materials 49, 290–299.

Shemtov-Yona, K., Rittel, D., 2015b. An overview of the mechanical integrity of dental implants. BioMed research international 2015.

Shemtov-Yona, K., Rittel, D., 2016a. Fatigue failure of dental implants in simulated intraoral media. Journal of the Mechanical Behavior of Biomedical Materials 62, 636–644.

Shemtov-Yona, K., Rittel, D., 2016b. Fatigue of dental implants: Facts and fallacies. Dentistry Journal 4 (2), 16.

Shemtov-Yona, K., Rittel, D., 2016c. Random spectrum loading of dental implants: An alternative approach to functional performance assessment. Journal of the mechanical behavior of biomedical materials 62, 1–9.

Shinjo, J., Umemura, A., 2011. Surface instability and primary atomization characteristics of straight liquid jet sprays. International Journal of Multiphase Flow 37 (10), 1294–1304.

Suresh, P., Rao, P. V., Deshmukh, S., 2002. A genetic algorithmic approach for optimization of surface roughness prediction model. International Journal of Machine Tools and Manufacture 42 (6), 675–680.

Taro, M., Chaise, T., Nélias, D., 2015. A methodology to predict the roughness of shot peened surfaces. Journal of Materials Processing Technology 217, 65–76.

Taylor, T. A., 1995. Surface roughening of metallic substrates by high pressure pure waterjet. Surface and Coatings Technology 76, 95–100.

VanKuiken Jr, L. L., Byrnes, L. E., Kramer, M. S., Jan. 10 1995. High pressure water jet method of blasting low density metallic surfaces. US Patent 5,380,564.

Wang, X., Feng, C., 2002. Development of empirical models for surface roughness prediction in finish turning. The International Journal of Advanced Manufacturing Technology 20 (5), 348–356.

Wenjun, G., Jianming, W., Na, G., 2011. Numerical simulation for abrasive water jet machining based on ale algorithm. The International Journal of Advanced Manufacturing Technology 53 (1), 247–253.

Xie, J., Rittel, D., 2017. Three-dimensional stochastic modeling of metallic surface roughness resulting from pure waterjet peening. International Journal of Engineering Science 120, 241 – 253.

Yoon, S., Hewson, J., DesJardin, P., Glaze, D., Black, A., Skaggs, R., 2004. Numerical modeling and experimental measurements of a high speed solid-cone water spray for use in fire suppression applications. International Journal of Multiphase Flow 30 (11), 1369–1388.